

Shape memory alloy CuAlBe strands subjected to cyclic axial loads

J.F. Beltran, C. Cruz, R. Herrera, O. Moroni*

Universidad de Chile, Facultad de Ciencias Físicas y Matemáticas, Beaucheff 850, Santiago, Chile

ARTICLE INFO

Article history:

Received 13 July 2010

Received in revised form

18 March 2011

Accepted 13 June 2011

Available online 16 July 2011

Keywords:

Shape memory alloys

CuAlBe alloy

Cables

Mechanical characterization

Damping capacity

ABSTRACT

Structural cables are composed of wires helically wound into strands, which, in turn, are wound around a core. They have high redundancy and can be used to carry large tensile forces in many civil engineering structures. Better dissipation and/or recentering capacity can be expected if the cable is composed of shape memory alloy (SMA) wires in the austenite phase. Tensile tests were performed on strands made of CuAlBe SMA wires to characterize their behavior and demonstrate their potential utility as adaptive or resilient tension elements. In particular, equivalent viscous damping and forward-transformation and maximum stresses were determined for different strain amplitudes. Nearly ideal superelastic properties were obtained up to 3% axial strain. The equivalent damping increased with strain, reaching a value of 4% for a strain amplitude of 5%. Strand experimental results were used to validate a two-dimensional numerical model developed to estimate the strand response to axisymmetric loads within the superelastic deformation range. The model relies on the linearization of the wire geometry and on a multilinear CuAlBe wire stress–strain relationship. The proposed model adequately predicts the maximum strand stress and the residual strains for different strain amplitudes.

© 2011 Elsevier Ltd. All rights reserved.

1. Introduction

Shape memory alloys (SMAs) are metallic alloys that are able to recover their original shape through a phase transformation in the material caused by the imposition of a temperature (shape memory effect) and/or stress field (pseudoelasticity or superelasticity). These unique thermomechanical properties have made SMAs a promising material for orthodontics, medical, and engineering applications. Basically, there are two phases associated with SMAs, namely the austenite phase and the martensite phase. Austenite is stable at high temperatures and low stresses whereas martensite is stable at low temperatures and high stresses. Four temperatures define the phase transformation limits: martensite start (M_s), martensite finish (M_f), austenite start (A_s), and austenite finish (A_f). Copper-based SMAs possess thermomechanical properties that make them ideal for energy dissipation and recentering devices for structural applications. However, adequate dissipation and recentering characteristics have only been achieved for small-diameter SMA wires and rods tested as single elements in tension, or in small-scale models tested in shaking tables [1–5]. Attempts to achieve the same characteristics for larger sizes required in real structures have been unsuccessful, due in part to the large variability in mechanical properties, depending on the manufacturer and thermal treatment used [6,7]. This variability makes it difficult to

define representative material properties, needed for the design of a real structure.

The use of structural cables made of small-diameter SMA wires seems to be an alternative application of this material to civil structures. Cables have high redundancy and can be used to carry large tensile forces. Improved dissipation and/or recentering capabilities can be expected, if the cable is formed by SMA wires in the austenite phase.

Few tests results have been reported in the literature on SMA cables subjected to axisymmetric loads. Reedlunn and Shaw [8] conducted experiments on two commercially available Nitinol cables. The specimens were uniaxially loaded in tension, and infrared imaging was used to monitor transformation activity. The elongation rate was rather low. The response qualitatively matches the typical behavior of NiTi wires when the helix angle is low, but it differs substantially for a larger helix angle. In the latter, the hysteresis boucles are rather small and so is the energy loss per cycle. Additionally, in both cases, residual deformations are apparent.

This paper presents results from experimental and numerical studies conducted on strands made of CuAlBe SMA wires. The objectives of these studies were to characterize the behavior of SMA strands and explore their potential utility as adaptive or resilient tension elements. Parallel and twisted strands were uniaxially loaded considering constant and variable strain amplitudes. Then, the equivalent viscous damping (ξ), and forward-transformation (σ_t) and ultimate (σ_u) stresses were determined from the stress–strain curves, for each maximum strain. In addition, strand experimental results were used to validate a two-dimensional (2D) analytical discrete model to estimate the cable

* Corresponding author.

E-mail address: mmoroni@ing.uchile.cl (O. Moroni).

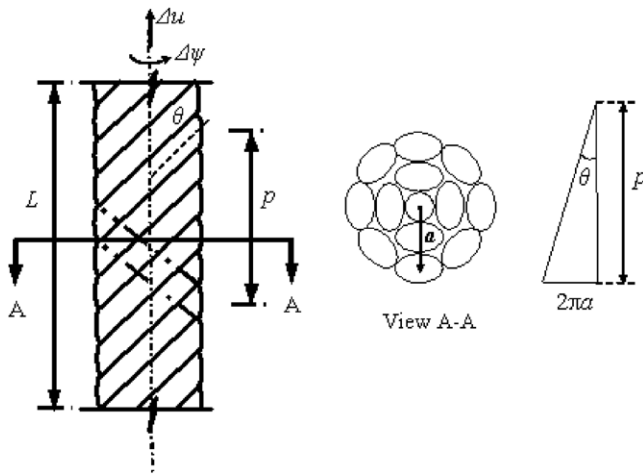


Fig. 1. Cable geometry.

response under axisymmetric loads. In this model, the wire geometry is linearized and, based on the work by Motahari and Ghassemieh [9], a multilinear CuAlBe SMA wire stress–strain curve was used for computational purposes. The original work by Motahari and Ghassemieh [9] was extended to include the residual deformation experienced by each CuAlBe SMA wire after each strain cycle. Comparisons were made between the responses of strands with parallel and twisted configurations, and between the responses of the strands and individual wire.

2. Cable characterization and modeling

A cable is a hierarchical structure constructed by wrapping in a helical fashion a group of thin wires around a single straight wire to form a strand. A group of strands is then laid helically around a straight core to form a cable (twisted wire cable). Strands can be wrapped around the core in concentric circles to form what it is called the layers of the cable. For a cable subjected to axisymmetric loads, it is assumed that the initial and deformed configurations of the wires can be described by a circular helix. Hence, three geometric parameters are needed to describe a wire configuration: the helix radius (a); the projected length of the rope component on the core axis (L); and the pitch distance (p), as shown in Fig. 1. The helix radius is the distance measured from the core axis to the centerline of the wire and the pitch distance of a wire is the distance along the core component, measured for a variation of a swept angle from 0 to 2π .

A cable can be a critical component in many engineering applications, including cranes, lifts, mine hoisting, bridges, electrical conductors, offshore mooring, and so on. Different classes of cables, suited for different purposes, have a different number and arrangement of rope elements within the cable cross-section, and the cable elements can be made of different materials. Each field of cable application has developed a specific body of knowledge, based on extensive testing and field experience, leading to empirical rules for each particular application. Unifying these empirical rules under some general mathematical and mechanics-based theory would allow a better understanding, and in the long term, a better prediction of the mechanical behavior of cables than current methods permit. In addition, a unified modeling approach can help reduce the need for expensive tests under a variety of operating conditions. Thus, due to their extensive use and the need to predict their behavior, several researchers have developed analytical models to estimate the cable response based on the material properties and the geometrical arrangement of the wires [10,11].

Several 2D mathematical models are currently available to predict the response of metallic and synthetic-fiber cables

subjected to axisymmetric loads. These models can be divided into two categories according to their formulation: discrete models, in which equations are established for each individual wire and then assembled to obtain the response of the cable; and semi-continuum models, in which each wire layer is replaced by a transversely isotropic layer. In this study, emphasis is placed on discrete models, which are the most commonly employed in numerical studies. According to Jolicoeur and Cardou [12] and Cardou and Jolicoeur [10], current discrete mathematical models for predicting metallic cable response can essentially be divided into two categories, depending on the types of hypotheses employed: (a) fiber models, in which the wires can develop only tensile forces [13–18]; and (b) rod models, which are an extension of the fiber model, in which the wires can develop tensile and shear forces, as well as bending and twisting moments [19–25].

A major contribution to discrete fiber models has been made by Leech [26,27], for the case of synthetic-fiber cables. This discrete fiber model considers the hierarchical structure of a cable's geometry, and it addresses the effects of frictional forces, transverse deformation of the cable cross-section, heat generation due to fiber hysteresis, and fatigue on the cable behavior [28]. Beltran and Williamson [29,30] have presented a discrete rod model to simulate synthetic-fiber cable responses under axial loads. This model relies on previous models by Costello [22] and Leech [27], but focuses on taking into account the degradation of mechanical cable properties as a function of loading history and estimating the effect of broken cable elements on the overall cable response.

3. SMA constitutive models

During the last two decades, a lot of research has been conducted to develop SMA constitutive models. Most of these models can be classified in the following two categories: micromechanics-based models and phenomenological models. Micromechanics-based models give a constitutive relation for a single grain and then, through the use of averaging techniques, the constitutive relations for a representative volume element (RVE) are obtained. Although these models provide valuable information about the phase transformation process, they require a large amount of numerical computation to be performed and they are not easily applicable at the structure level. Thus, the use of such models to estimate the overall response of SMA structures is limited (see, among others, [31–33]). Phenomenological models are built on the principles of thermodynamics with internal variables to describe the material behavior and/or direct curve fitting of experimental data. These models are quite accurate in predicting the uniaxial response of SMAs and can be easily integrated into numerical algorithms developed to analyze structural systems (e.g. the finite element method) (see, among others, [34–37]).

4. Experimental procedure and results

Four 15 cm long strand specimens were constructed from 0.5 mm diameter CuAlBe wires, furnished by Trefimétaux, France. The nominal composition of the wires was Cu–11.8 wt%Al–0.5 wt%Be. The phase transformation temperatures reported by the manufacturer were $M_f = -47$ °C, $M_s = -18$ °C, $A_s = -20$ °C, and $A_f = 2$ °C. Since ambient temperatures for civil engineering structures are usually greater than the A_f transition temperature of 2 °C, the material was expected to operate within its superelastic range.

Based on previous research [1], it was decided to heat the wires at 700 °C for 20 s, which resulted in a nominal grain size of 60 μm , as shown in Fig. 2. Two specimens were formed by 6 wires wrapped around a single straight wire, followed by 12 wires

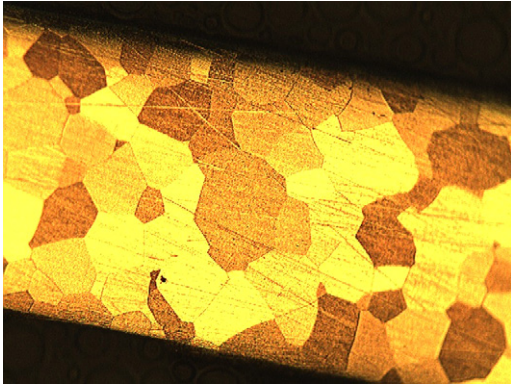


Fig. 2. Micrograph of a specimen heated at 700 °C during 20 s.

wrapped around them. The nominal outer diameter was 2.5 mm. The helix angle of the exterior wires was 17.5°. The other two specimens were made using the same number of wires, but in parallel. No thermal treatment was applied after manufacturing the specimens, to avoid any grain size increase.

The four strands were tested under cyclic tension at the Structural Engineering and Material Research Laboratory, Georgia Institute of Technology. The specimens were uniaxially loaded by an MTS electromechanical load frame, using a 250 kN load cell to monitor the force, while the grip displacement was measured by an internal linear variable differential transformer (LVDT), as shown in Fig. 3. The strand elongation was estimated from the grip displacement, considering that the compliance of the testing machine accounted for less than 0.1% of this value.

Two patterns of controlled displacements were applied, based on an equivalent strain level calculated as the total elongation of the strand divided by the initial distance between the grips. The first pattern, of 20 cycles at 2% equivalent strain amplitude, was followed by the second pattern of 22 cycles with increasing equivalent strain amplitudes varying from 0.5% to 8%, applied in the following sequence: 3 cycles at 0.5%, 1 cycle at 0.8%, 1.0%, and 1.5%, 5 cycles at 2.2%, 1 cycle at 2.5%, 3.0%, 3.5%, 4.0% and 4.5%, 5 cycles at 5.0%, and 1 cycle at 8.0%. The second pattern was used to determine the superelastic limit and the effect of previous deformation. The equivalent strain rate was 0.1 mm/s. For all specimens, the initial distance between the grips was about 10 cm, at zero load. All tests were performed at room temperature.

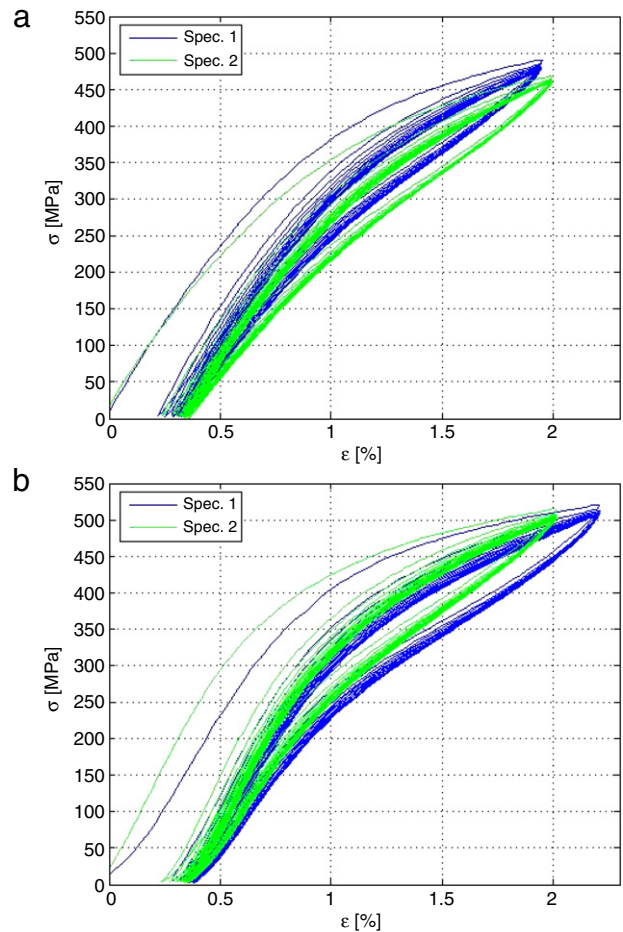


Fig. 4. Stress–strain curves. 20 cycles at 2% strain (a) twisted strand, (b) parallel strand.

Fig. 4 shows equivalent stress–strain relationships for the twisted and the parallel strands subjected to the first pattern of deformation. The equivalent stress developed by each strand specimen was calculated as P/A_0 , where P is the axial load on the strand and A_0 is the initial area of the total number of wires conforming the strand. The equivalent stress–strain curves in Fig. 4

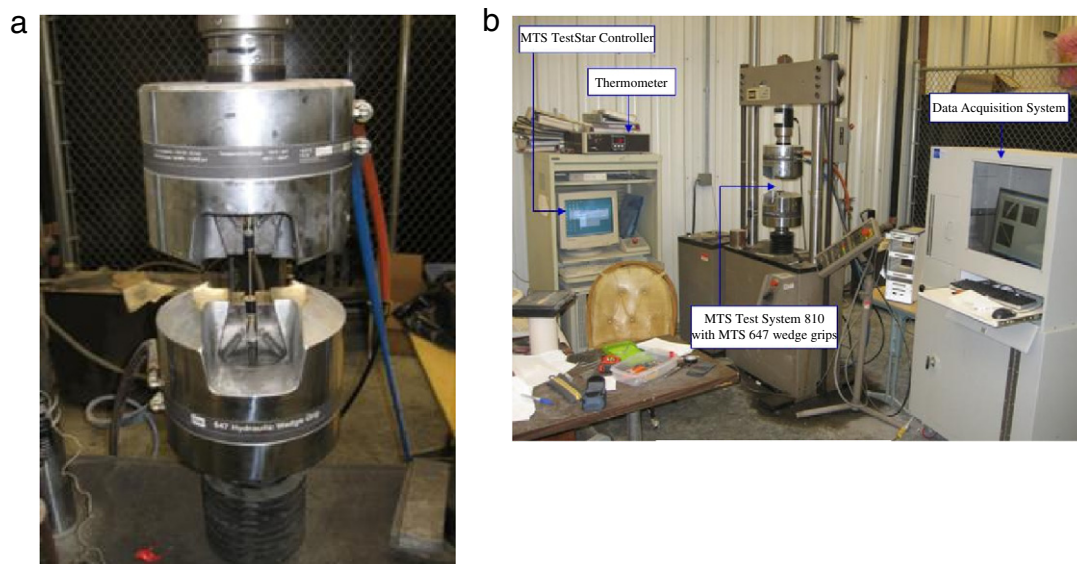


Fig. 3. Experimental setup.

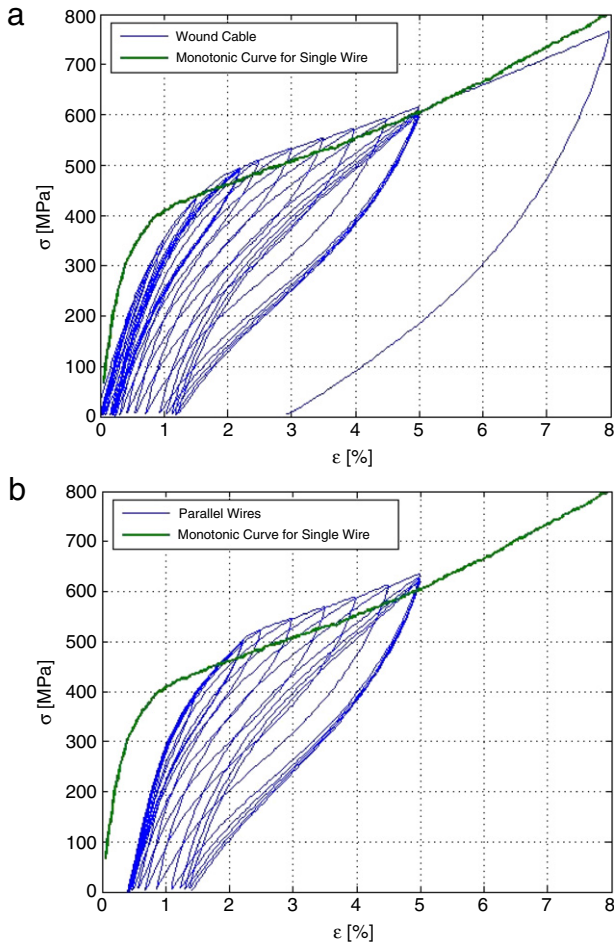


Fig. 5. Strand response for increasing strain amplitudes and single wire response (a) twisted strand, (b) parallel strand.

are quite similar, and resemble the response of a single wire, presented in a previous work [1]. The first cycle was somewhat different from the others, while all the rest were very close to each other. This effect, dubbed “training” by previous researchers [38], has been observed in tests of individual wires as well [1,6].

Fig. 5 shows the curves for the second pattern of deformation, with the monotonic curve obtained for a single wire tested at 25 °C overlaid on top. The second pattern was applied to the parallel strand immediately after the first pattern; that explains the offset in Fig. 5(b). As is expected for CuAlBe polycrystal samples, no distinct plateau is visible; instead, a slightly positive tangent stiffness is apparent. The residual deformations are smaller than those reported by Reedlunn and Shaw [8] for NiTi cables. No difference between the first cycle and the others can be noticed up to 2.2%, due to the previous training imposed by the constant equivalent strain amplitude tests. This is not the case for strains larger than that previous limit.

Table 1 shows the equivalent elastic modulus, E , forward transformation stress, σ_t , and maximum tensile stress, σ_{max} , for the four strands, calculated from the experimental results, and for a single wire, reported by Marivil [39]. All the parameters have been determined excluding the first cycle. The equivalent elastic modulus of the strands and the wire decreases as the strains get larger. Experimental results confirm that larger equivalent elastic modulus and transformation stresses can be expected for the parallel strand compared to the twisted strand, due to the inclination of the wires in the latter. The single wire and strand properties have similar values for similar nominal strains.

5. Analytical model

5.1. Cable response model

As previously stated, for modeling purposes it is assumed that the initial and deformed configuration of a thin wire can be described by a circular helix. By definition, a circular helix curve maintains a constant angle (helix angle) with a fixed line in space. This fixed line is the longitudinal axis of the strand, and the helix angle θ is defined as the angle between the axis of the component and the axis of the core component (Fig. 1). The helix angle θ can be computed using the following expression:

$$\tan(\theta) = \frac{2\pi a}{p} \quad (1)$$

Due to its helical nature, a twisted wire cable possesses nonlinear strain–displacement relationships, and its axial behavior exhibits coupling between tension and torsion. Some researchers [24,40], however, have validated the use of the linearized version of the theory to estimate the cable response under axisymmetric loads. The linearized theory is based on the linearization of the strain–displacement relationships of a cable component and the components’ constitutive laws, and on the use of the initial cable configuration as the reference configuration. The validation procedure was performed using comparisons among different linear models [12,24], nonlinear models [24,41], and experimental data on steel wire cables and polyester ropes. After extensive parametric studies on cables with different geometric parameters and with linear and nonlinear constitutive laws, it was concluded that linear models (fiber and rod models) are quite satisfactory to estimate the overall cable response (cable stiffness, breaking axial load, and breaking axial strain) for cables with helix angle less than 20° having both ends restricted to rotation [40].

The linearized relationship of the wire axial strain ε_i in terms of the cable axial strain ε and the angle of twist per unit length φ is given by ([17,18])

$$\varepsilon_i = \varepsilon \cos^2 \theta_{0i} + \varphi a_{0i} \cos \theta_{0i} \sin \theta_{0i}, \quad (2)$$

where a_{0i} and θ_{0i} are the helix radius and the helix angle of wire i , respectively. As such, the linearized overall behavior of a cable subjected to axisymmetric loading can be written in the following incremental form:

$$\begin{pmatrix} \Delta F \\ \Delta M \end{pmatrix} = \begin{bmatrix} F_\varepsilon & F_\varphi \\ M_\varepsilon & M_\varphi \end{bmatrix} \cdot \begin{pmatrix} \Delta \varepsilon \\ \Delta \varphi \end{pmatrix}, \quad (3)$$

where F_ε , F_φ , M_ε , and M_φ are the tangent stiffness coefficients; ΔF and ΔM are the increments in axial force and axial moment (torsion), respectively; and $\Delta \varepsilon$ and $\Delta \varphi$ are the increments in axial deformation and axial rotation per unit length, respectively. The axial strains are defined as follows. $\Delta \varepsilon = \Delta u/L$ and $\Delta \varphi = \Delta \psi/L$, where Δu and $\Delta \psi$ are the axial displacement and axial rotation, respectively (Fig. 1), and L is the initial cable length. Considering the fiber model, the tangent stiffness coefficients have the following form [12]:

$$F_\varepsilon = (AE)_c + \sum_{i=1}^n (AE)_i \cos^3 \theta_{0i} \quad (4a)$$

$$F_\varphi = M_\varepsilon + \sum_{i=1}^n (AE)_i a_{0i} \cos^2 \theta_{0i} \sin \theta_{0i} \quad (4b)$$

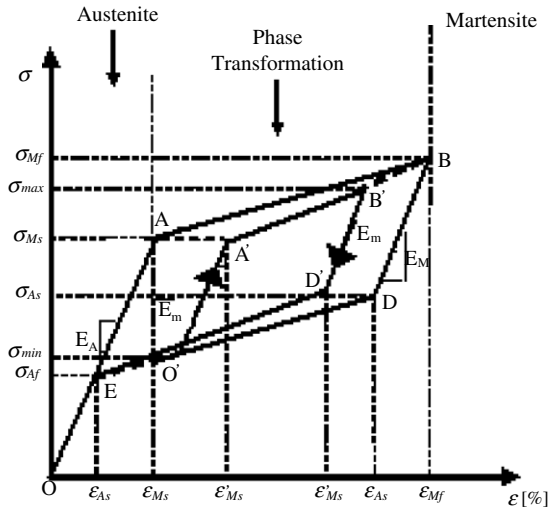
$$M_\varphi = (GJ)_c + \sum_{i=1}^n (AE)_i a_{0i}^2 \cos \theta_{0i} \sin^2 \theta_{0i}, \quad (4c)$$

where the subscript c refers to the cable core; $(AE)_i$ is the axial stiffness of wire i , with A_i being the cross-sectional area and E_i , defined as $(d\sigma/d\varepsilon)_i$, being the tangent modulus of wire i for a given wire axial deformation ε_i .

Table 1

Equivalent elastic modulus (E), forward transformation stress (σ_t), and maximum stress (σ_{\max}) determined from the experimental results.

Specimen type	Strain amplitude (%)	E_1 (GPa)	E_2 (GPa)	σ_{t1} (MPa)	σ_{t2} (MPa)	$\sigma_{\max 1}$ (MPa)	$\sigma_{\max 2}$ (MPa)
Twisted strand	2.0	51.7	51.5	255.5	205	477.5	460.8
Parallel strand	2.0	56.2	59.5	291.7	287.4	506.7	501.2
Twisted strand	5.0	38.3	41.3	207.2	218.4	551.4	605.8
Parallel strand	5.0	45.5	47.4	275	305.4	635.1	594.8
Wire	0.8		99.0		300.0		441.0
Wire	1.5		79.0		270.0		493.0
Wire	2.2		52.0		240.0		546.0

**Fig. 6.** Constitutive law of CuAlBe SMA wires.

5.2. Constitutive law of SMA wires

One of the phenomenological models available in the literature is the model developed by Motahari and Ghassemieh [9]. This model was used in this research due to its easy implementation in a numerical model because it establishes a multilinear one-dimensional constitutive law to predict the behavior of SMA wires under different loading conditions (Fig. 6). This model is described by the following parameters: austenite elastic stiffness E_A ; martensite elastic stiffness E_M ; martensite start critical stress σ_{Ms} ; martensite finish critical stress and strain (σ_{Mf} , ε_{Mf}); austenite start critical strain ε_{As} ; and the austenite finish critical stress and strain at the end of the reverse transformation (σ_{Af} , ε_{Af}). These parameters are obtained from experimental SMA wire data. The stress–strain relationships on different paths in Fig. 6, which simulate the pseudoelastic behavior of SMAs, are defined as follows.

Paths $O-A$ and $E-O$ (elastic–fully austenite)

$$\sigma = E_A \varepsilon. \quad (5)$$

Path $A-B$ (forward transformation)

$$\sigma = \sigma_{Ms} + \frac{\sigma_{Mf} - \sigma_{Ms}}{\varepsilon_{Mf} - \varepsilon_{Ms}} (\varepsilon - \varepsilon_{Ms}). \quad (6)$$

Path $B-D$ (fully martensite)

$$\sigma = \sigma_{Mf} + E_M (\varepsilon - \varepsilon_{Mf}). \quad (7)$$

Path $D-E$ (reverse transformation)

$$\sigma = \sigma_{As} + \frac{\sigma_{Af} - \sigma_{As}}{\varepsilon_{Af} - \varepsilon_{As}} (\varepsilon - \varepsilon_{As}). \quad (8)$$

According to Motahari and Ghassemieh [9], if the unloading occurs before the completion of the forward transformation or the

reloading starts before completion of the reverse transformation, then the elastic stiffness is different from both the austenite and martensite phase stiffnesses (paths $O'-A'$, $A'-B'$, $B'-D'$ and $D'-O'$). The authors proposed the following expression to estimate the tangent stiffness E_m (Fig. 6):

$$E_m = \frac{E_M E_A}{x (E_A - E_M) + E_M}, \quad (9)$$

where x is defined as $(\varepsilon_{\max} - \varepsilon_{Ms}) / (\varepsilon_{Mf} - \varepsilon_{Ms})$ for the unloading case and $(\varepsilon_{\min} - \varepsilon_{As}) / (\varepsilon_{As} - \varepsilon_{Af})$ for the loading case. ε_{\max} and ε_{\min} are the maximum and minimum strains before unloading or reloading, respectively.

It has been reported that copper-based SMAs develop residual strains when subjected to cyclic loading (partial pseudoelastic behavior), even if the temperature is greater than A_f and the amplitude of the strain is less than the superelastic limit [1]. Accordingly, the multilinear model proposed by Motahari and Ghassemieh [9] was modified to include the residual strain developed by each SMA wire after each cycle.

The residual strain in the SMA wire after cycle i , $(\delta_\varepsilon)_i$, is considered to be a fraction (η_i) of the maximum amplitude $(\varepsilon_{\max})_i$ of the corresponding cycle i as follows:

$$(\delta_\varepsilon)_i = \eta_i \cdot (\varepsilon_{\max})_i. \quad (10)$$

Based upon the experimental results of the current research, the rate of residual strain, η_i , after cycle i is assumed to have an exponential evolution in the following form:

$$\eta_i = A \cdot e^{-\lambda \cdot i}, \quad (11)$$

where A and λ are parameters obtained from experimental data. Using the experimental data shown in Fig. 5, the values of the parameters A and λ are 0.027 and 0.4474, respectively. Therefore, considering a linear accumulation rule, the total (accumulated) residual strain in the strand, after the end of cycle i , is given by

$$(\varepsilon_R)_i = \sum_{k=1}^i (\delta_\varepsilon)_k. \quad (12)$$

The multilinear constitutive law is displaced in the positive strain (ε) axis of the plane $\sigma-\varepsilon$, after each cycle, by an amount equal to the corresponding residual strain (Eq. (9)). Thus, for any given cycle, all the characteristic strains ε_x (i.e. ε_{Ms} , ε_{Mf} , ε_{As} , ε_{Af}) must be recalculated for the next cycle as

$$\varepsilon'_x = \varepsilon_x + \varepsilon_R. \quad (13)$$

For the assignment of the tangent modulus, three possible scenarios are considered (Fig. 7). The first scenario (Fig. 7(b)) considers that the unloading occurs before the strain reaches ε_{Ms} . No residual strains are developed in this case, because the material response is within the linear elastic range. The second scenario Fig. 7(c) assumes that the unloading occurs after the strain reaches ε_{Ms} , but before the stress, σ_{\max} , in the strand elements (i.e. wires) reaches σ_{As} . The tangent stiffness E_{24} is the slope of the straight line connecting points F and D . The value of the unloading strain at the end of the reverse transformation considering residual strain, ε_{AfR} , is obtained by intersecting the unloading path $F-D$ with a line

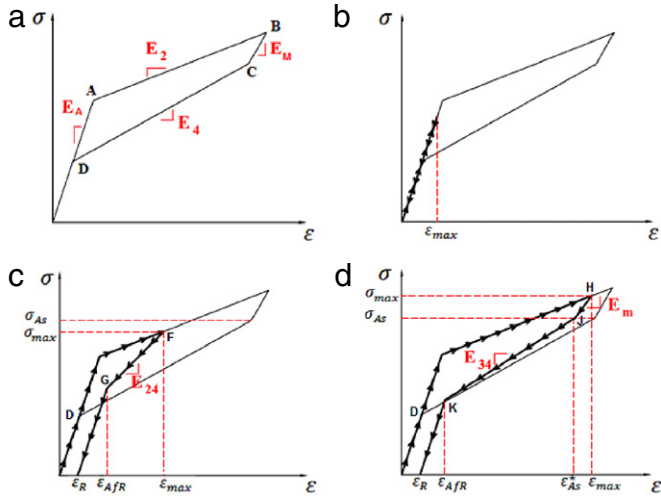


Fig. 7. Model to consider residual strains.

parallel to OD starting from \$\epsilon_R\$. The parameters \$E_{24}\$, \$\epsilon_{AFR}\$, and \$\sigma_{max}\$ can be calculated using the following expressions:

$$E_{24} = \frac{\sigma_{max} - \sigma_{Af}}{\epsilon_{max} - \epsilon_{Af}} \quad (14)$$

$$\epsilon_{AFR} = \frac{E_A \cdot \epsilon_R + \sigma_{Af} - E_{24} \cdot \epsilon'_{Af}}{E_A - E_{24}} \quad (15)$$

$$\sigma_{max} = \sigma_{Mf} - E_2 \cdot (\epsilon'_{Mf} - \epsilon_{max}). \quad (16)$$

The last case (Fig. 7(d)) considers that unloading occurs after the stress in the cable reaches \$\sigma_{As}\$. In this case, while the stress in the strand element (wire) is above \$\sigma_{As}\$ (path H–J in Fig. 7(d)), the tangent stiffness \$E_m\$ is assigned using Eq. (8). Once the stress in the wire is equal to or smaller than \$\sigma_{As}\$, the tangent stiffness \$E_{34}\$ is the slope of the line JD, and the strain at the end of the reverse transformation considering residual strain \$\epsilon_{AFR}\$ is computed by intersecting the unloading path J–K with a line parallel to OD starting from \$\epsilon_R\$. The value of \$\sigma_{max}\$ is computed using Eq. (16), and the parameters \$E_{34}\$ and \$\epsilon_{AFR}\$ can be calculated using the following expressions:

$$E_{34} = \frac{\sigma_{As} - \sigma_{Af}}{\epsilon_{As}^* - \epsilon'_{Af}} \quad (17)$$

$$\epsilon_{AFR} = \frac{E_A \cdot \epsilon_R + \sigma_{Af} - E_{34} \cdot \epsilon'_{Af}}{E_A - E_{34}}, \quad (18)$$

where

$$\epsilon_{As}^* = \epsilon_{max} - \frac{(\sigma_{max} - \sigma_{As})}{E_m}. \quad (19)$$

It is envisioned that the applications of CuAlBe strands will be restricted to the superelastic response; thus the proposed analytical model has been validated within this range of deformation.

6. Results and discussion

In Fig. 8, comparisons between experimental data and predicted strand responses (based on the proposed analytical model) are presented for the twisted wire configurations for both patterns of controlled displacements up to 2% strain. The parameters used to define the constitutive law of CuAlBe SMA wires are the following (Fig. 6): \$E_A = 57,000\$ MPa; \$E_M = 32,633\$ MPa; \$\sigma_{Ms} = 340\$ MPa; \$\sigma_{Mf} = 580.5\$ MPa; and \$\sigma_{Af} = 180\$ MPa. These parameters were obtained from the parallel strand tests. The value of \$E_A\$ is the

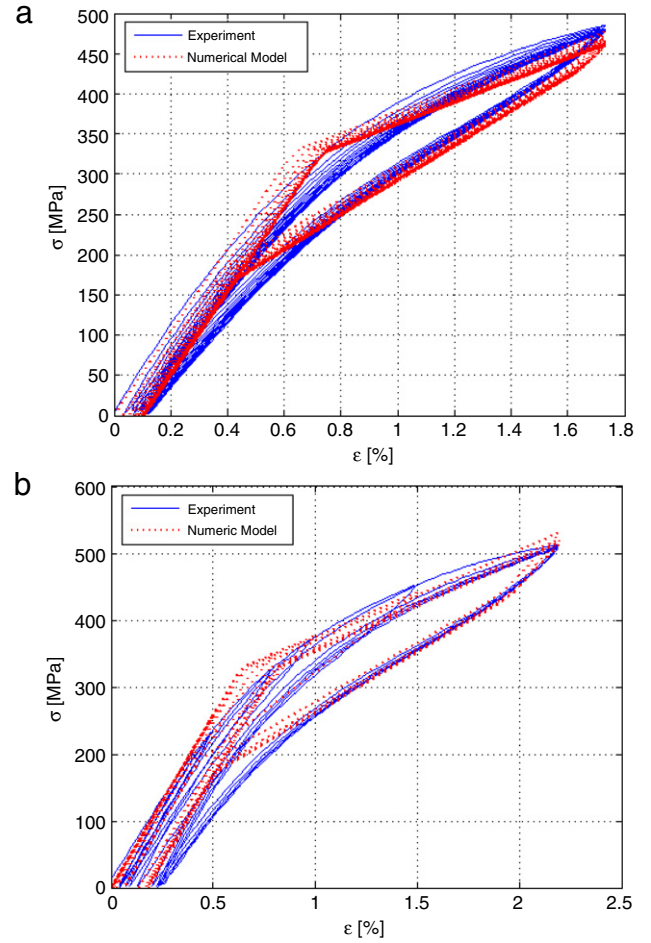


Fig. 8. Experimental and predicted responses for twisted strand (a) constant strain amplitude, (b) increasing strain amplitude.

average of the austenite elastic stiffness considering both parallel strand tests, while the rest of the parameters were calibrated using the data of one parallel strand because one wire of the other strand failed during the test at constant strain amplitude. The slope between the stresses \$\sigma_{Ms}\$ and \$\sigma_{Mf}\$ was obtained by a linear regression analysis of measurements on the strain interval [1%, 2%] enforcing that the maximum stress measured belonged to this curve. The value of \$\sigma_{Ms}\$ was calculated by intersecting the curve between stresses \$\sigma_{Ms}\$ and \$\sigma_{Mf}\$ and the elastic path OA (Fig. 6). The slopes \$E_M\$ (curve B–D) and between stresses \$\sigma_{Ms}\$ and \$\sigma_{Af}\$ (curve D–E) were also obtained by linear regression analyses considering strains in the ranges [1.5%, 2%] and [0.5%, 1.5%], respectively (Fig. 6). The value of the stresses \$\sigma_{As}\$ and \$\sigma_{Af}\$ were computed by intersecting the curves B–D and D–E and D–E and O–A, respectively. The numerical simulations overestimate the strand response (stress–strain curves) by no more than 20% for both types of strain pattern. This behavior is due to the fact that the multilinear one-dimensional constitutive model selected for numerical simulations is not effective in fully capturing the nonlinear CuAlBe strand response. The proposed model, however, adequately predicts the maximum strand axial stress, the equivalent viscous damping, and the residual strain at each strain cycle, as discussed with respect to subsequent figures (Figs. 9 and 10).

The values of the equivalent viscous damping, \$\zeta\$, for both strand types and individual wires, considering test results and numerical simulations, are shown in Fig. 9 as a function of the maximum equivalent strain amplitude. This parameter is calculated as the energy loss per cycle divided by \$4\pi\$ times the secant elastic strain

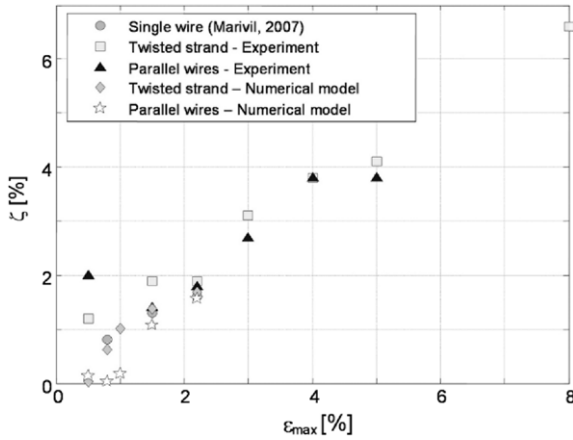


Fig. 9. Equivalent viscous damping versus strain.

energy per cycle. For all the cases analyzed, the equivalent viscous damping values increase with increasing levels of maximum strain. The maximum value of ζ is equal to 4%, reached at a maximum strain equal to 5%, which is considered a moderate value. The predicted values are comparable to the experimental values for strains larger than 1%, with errors between 10% and 20% with respect to the experimental values, for both types of strand configuration. For strains below 1%, the numerical model predicts very low equivalent viscous damping values due to the flag-shaped constitutive model of the SMA used in this research, whereby the predicted strand response is basically elastic for low strains.

The variations of the equivalent elastic modulus, residual strain, and maximum strain with respect to the maximum strain at each cycle for both types of strand configuration are shown in Fig. 10. Numerical simulations show that the equivalent elastic modulus of the twisted strands is smaller than the equivalent elastic modulus of the parallel strands (52 GPa and 58 GPa, respectively), and their values remain nearly constant for equivalent strain amplitudes up to 2.2%. This conclusion is supported by the experimental data (Fig. 10(a)), which shows that the equivalent elastic modulus of both types of strand configuration remain constant up to a maximum strain of 3%. For this strain range, variations of the predicted values with respect to the average experimental values are found to be no more than 4% for the twisted strand configuration and 1% for the parallel strand configuration. For larger values of the maximum strain, the equivalent elastic modulus decreases, which indicates that the martensite phase is increasingly retained after unloading. Thus, it may be concluded that the strands have pseudoelastic behavior up to maximum equivalent strain amplitudes of 3%. Moreover, the residual strains increase as the maximum equivalent strain amplitudes get larger (Fig. 10(b)), but, for values below 3%, the residual strains are smaller than 0.5%, which corroborates the fact that a maximum strain of 3% may be considered as the limit of superelastic behavior. The predicted values of residual strains compare quite well with experimental data (error with respect to experimental data less than 2%) for both types of strand configuration. In Fig. 10(c), comparisons between predicted and measured maximum stress values for increasing strain cycles for both types of strand configuration are presented. The strain cycle values vary from 0.5% to 2.2%, values

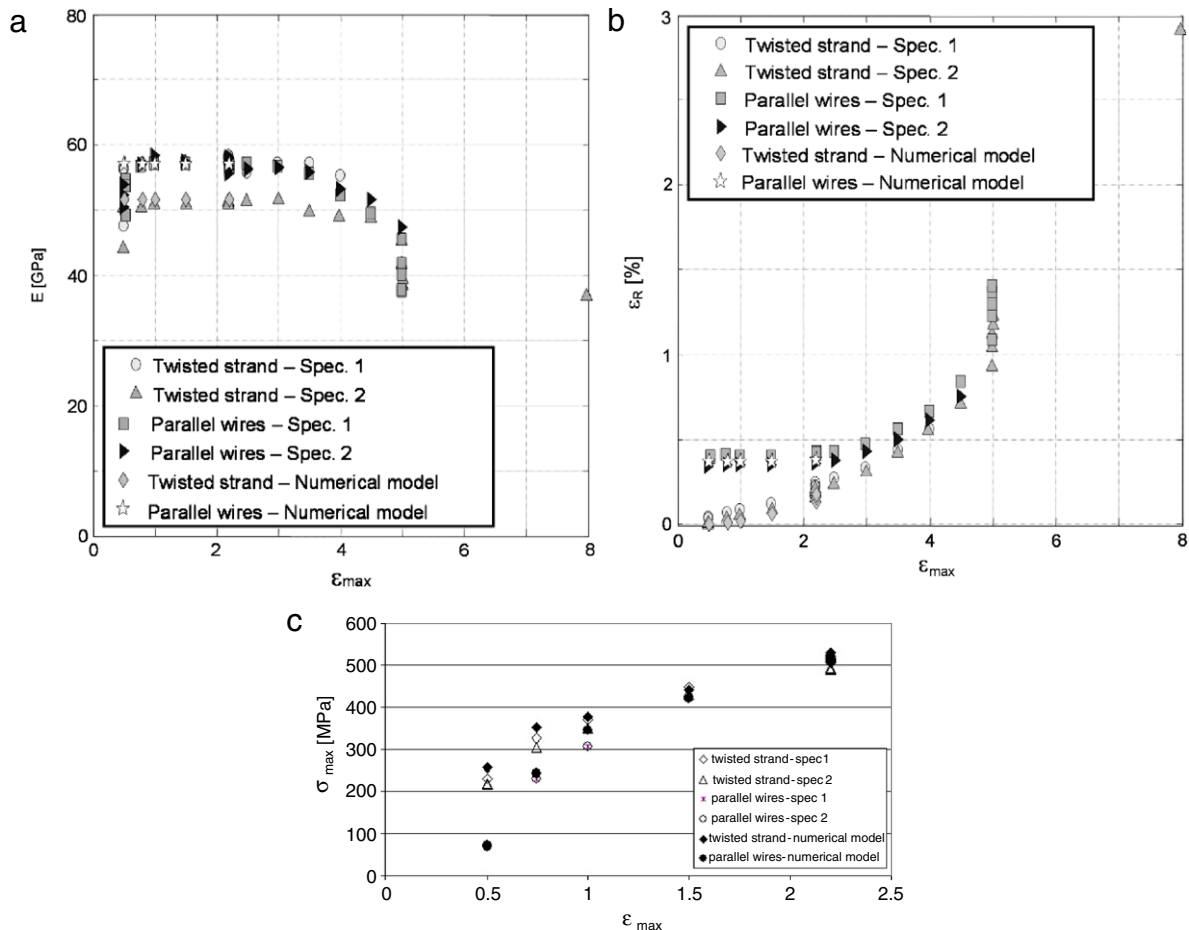


Fig. 10. Modulus of elasticity, residual strain, and maximum stress versus maximum strains (a) elastic modulus, (b) residual strain, (c) maximum stress.

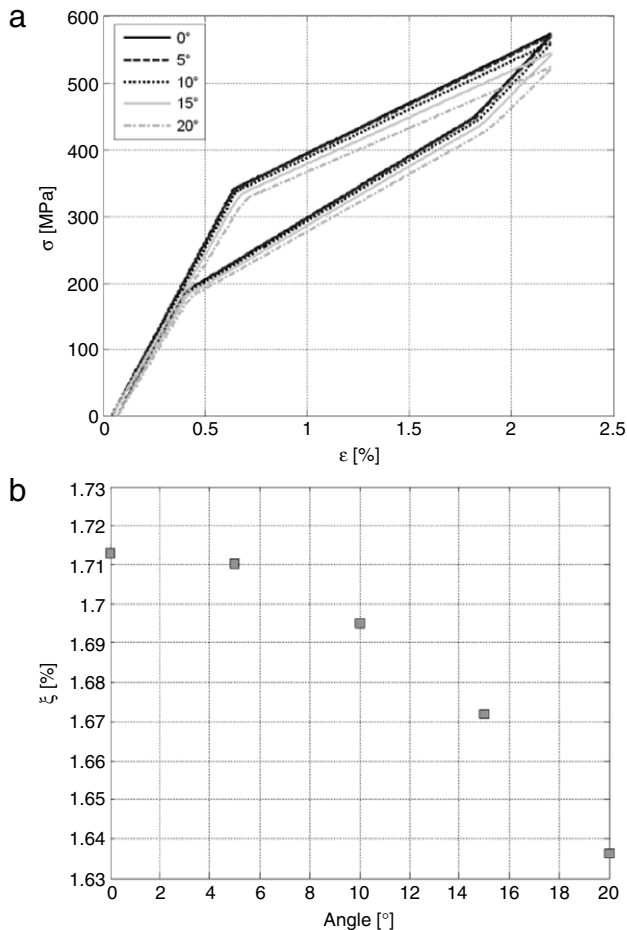


Fig. 11. Stress–strain curves and equivalent damping values from parametric analysis (a) stress–strain curves, (b) equivalent damping.

that are within the superelastic range of the strands previously defined. As the values of the strain cycle increase, the predicted and measured maximum stress values at each strain cycle increase as well. The predicted values of the maximum stress overestimate the experimental values by 1–7% for strains greater than 1% and by 2–20% for strains less than 1% relative to the experimental values. The increase of the range of variation for smaller strains is associated to the limitations of the constitutive model previously discussed.

Based on the numerical formulation of the proposed model, some of the variables that characterize strand response are the stress–strain cycles, the martensite start critical stress σ_{Ms} , and the equivalent viscous damping value. As such, using the proposed numerical model, parametric analyses are performed to study the dependence of these variables on the strand configuration. To show the capabilities of the proposed numerical model, in this paper, only the helix angle of the strand was varied to obtain different strand configurations, keeping other variables such as the number of wires, wire radius, and strand cross-section configuration constant. For this particular analysis, the helix angle of the strand ranges from 0° to 20°, and the numerical simulation curves presented in Fig. 11(a) were computed for a fixed equivalent strain amplitude of 2.2% using the same law for the rate of residual strain as in Fig. 8. As the helix angle of the strand increases, the strand response gets more flexible; the maximum stress developed by the strand decreases up to 8% and the strain at which the austenite–martensite transformation begins increases by approximately 25% with respect to the parallel configuration strand (0° in Fig. 11(a)). In addition, the energy loss per cycle and

equivalent viscous damping values diminish slightly as the helix angle gets larger. In the particular case of the viscous damping parameter (Fig. 11(b)), their values did not decrease more than 5% with respect to the value associated to the parallel strand configuration for the entire range of helix angle considered.

7. Conclusions

CuAlBe twisted and parallel strands were tested in tension, and their mechanical characteristics were determined. An analytical 2D model, developed by previous researchers, was extended in order to simulate the CuAlBe strand response under cyclic tension. This model was calibrated to reproduce the strand response within the superelastic deformation range.

Strand equivalent stress–strain cycles showed similar behavior to those obtained from a single wire. For each equivalent strain amplitude, the hysteretic response stabilized after the first cycle. A superelastic limit of 3% was determined based on the variation of the strand stiffness and residual deformations. The equivalent viscous damping increased with equivalent strain amplitude, reaching a value of 4% for strains of 5%, which is considered a moderate value.

According to the comparisons presented in this research between predicted and experimental values, the proposed analytical model adequately predicts, for both types of strand configuration, the maximum stresses developed, residual strains, equivalent elastic modulus, and equivalent viscous damping values for the different equivalent strain amplitudes considered within the superelastic range of deformation. Although the equivalent viscous damping decreases for larger helix angles, from a practical point of view that loss is irrelevant compared to the advantage of handling a twisted strand. Additional analyses, however, especially on the evolution law that describes the accumulation of CuAlBe wire residual strain after each cycle and the constitutive model selected for CuAlBe wires that consider strains beyond the superelastic limit, are needed to validate the numerical model. The size of the wires used to fabricate the strands tested in this study is comparable to the size used to fabricate actual cables. Therefore, the behavior of larger cables and strands may be studied analytically, using the model proposed and calibrated in this research, and conclusions regarding energy dissipation, maximum stresses, and residual deformations can be obtained. However, these conclusions will need to be validated against experimental data for full-size specimens, which are currently unavailable.

There are a number of additional challenges that must be overcome before going to an actual application, including fabrication issues, such as the process of twisting and heat treating the cable, cost issues, and fatigue and fracture issues. They have not been addressed in this work, considering that this is a first approach to assess the feasibility of using these cables.

Acknowledgments

This research has been funded by University of Chile (Program for short visit of graduate students) and FONDECYT (grants no 1070370 and 7070265). Special thanks go to Dr. Reginald DesRoches for providing the facilities to conduct the tests at Georgia Institute of Technology.

References

- [1] Araya R, Marivil M, Mir C, Moroni MO, Sepúlveda A. Temperature and grain size effects on the behavior of CuAlBe SMA wires under cyclic loading. *Mater Sci Eng A* 2008;6(6):725–801.
- [2] Sepúlveda J, Boroschek R, Herrera R, Moroni MO, Sarrazin M. Steel beam–column connection using copper-based shape memory alloy damper. *J Constr Steel Res* 2008;64:429–35.

- [3] Herrera R, Moroni MO, Olea M, Sarrazin M. Prestressed beam-to-column moment connections using Cu-based SMA rods. Proc 9NCEE, (2010), paper 1340.
- [4] Boroschek R, Farias G, Moroni MO, Sarrazin M. Effect of SMA braces in a steel frame building. J Earthquake Eng 2007;11(3):326–42.
- [5] Casciati F, Faravelli L. A passive control device with SMA components: from the prototype to the model. Struct Control Health Monit 2009;16:751–65.
- [6] Casciati F, Van der Eijk. Variability in mechanical properties and microstructure characterization of CuAlBe shape memory alloys for vibration mitigation. Smart Struct Syst 2008;4(2):103–21.
- [7] Torra V, Isalgue A, Martorell F, Terriault P, Lovey FC. Built in dampers for family homes via SMA: an ANSYS computation scheme based on mesoscopic and microscopic experimental analyses. Eng Struct 2007;29:1889–902.
- [8] Reedlunn B, Shaw J. Shape memory alloy cables. Behav Mech Composite Mat SPIE 2008;6928.
- [9] Motahari S, Ghassemieh M. Multilinear one-dimensional shape memory material model for use in structural engineering applications. Eng Struct 2007;29:904–13.
- [10] Cardou A, Jolicoeur C. Mechanical models of helical strands. Appl Mech Rev 1997;50(1):1–14.
- [11] Ghoreishi S, Messenger T, Cartraud P, Davies P. Validity and limitations of linear analytical models for steel wire strands under axial loading, using 3D FE model. Int J Mech Sci 2007;49:1251–61.
- [12] Jolicoeur C, Cardou A. A numerical comparison of current mathematical models of twisted wire cables under axisymmetric loads. J Ener Res Tech 1991;113:241–9.
- [13] Hruska FH. Calculation of stresses in wire ropes. Wire and Wire Prod 1951;26:766–7. 799–801.
- [14] Hruska FH. Radial forces in wire ropes. Wire and Wire Prod 1952;27:459–63.
- [15] Hruska FH. Tangential forces in wire ropes. Wire and Wire Prod 1953;28:455–60.
- [16] Knapp RH. Nonlinear analysis of a helically armored cable with nonuniform mechanical properties. In: IEEE Ocean Conference; 1975. p. 155–64.
- [17] Knapp RH. Derivation of a new stiffness matrix for helically armoured cables considering tension and torsion. Int J Num Meth Eng 1979;14:515–29.
- [18] Lanteigne J. Theoretical estimation of the response of helically armored cables to tension, torsion and bending. J Appl Mech 1985;52:423–32.
- [19] Machida S, Durelli AJ. Response of a strand to axial and torsional displacements. J Mech Eng Sci 1973;15:241–51.
- [20] Phillips JW, Costello GA. Contact stresses in twisted wire cables. J Eng Mech Div 1973;99:331–41.
- [21] Costello GA, Butson GJ. Simplified bending theory for wire rope. J Eng Mech Div 1982;108(2):219–27.
- [22] Costello GA. Stresses in multilayered cables. J Ener Res Tech 1983;105:337–40.
- [23] Velinsky SA, Anderson GL, Costello GA. Wire rope with complex cross sections. J Eng Mech 1984;110(3):380–91.
- [24] Velinsky SA. General nonlinear theory for complex wire rope. Int J Mech Sci 1985;27:497–507.
- [25] Jiang W. General formulation on the theories of wire ropes. J Appl Mech 1995;62:747–55.
- [26] Leech CM. Theory and numerical methods for the modeling of synthetic ropes. Comm Appl Num Meth 1987;3:407–713.
- [27] Leech CM. The modeling of friction in polymer fibre ropes. Int J Mech Sci 2002;44:621–43.
- [28] Banfield S, Hearle JWS, Leech CM, Lawrence CA. Fiber rope modeler: a cad program for the performance prediction of advanced cords and ropes under complex loading environments. Techtextil 2001.
- [29] Beltran JF, Williamson EB. Investigation of damage-dependent response of mooring ropes. J Eng Mech 2009;135(12):1237–47.
- [30] Beltran JF, Williamson EB. Numerical simulation of damage localization in polyester mooring ropes. J Eng Mech 2010;136(8):945–59.
- [31] Patoor E, Eberhardt A, Berveirler M. Micromechanical modeling of superelasticity in shape memory alloys. M. J Phys IV 1996;6: C1-277–C1-292.
- [32] Zhu J, Liang N, Huang W, Liew K, Liu Z. A thermodynamics constitutive model for stress induced phase transformation in shape memory alloy. Int J Solid Struct 2002;39:741–63.
- [33] Blanc P, Lexcelent C. Micromechanical modeling of a CuAlNi shape memory alloy behavior. Mat Sc Eng A 2004;378:465–9.
- [34] Graesser EJ, Cozzarelli FA. Shape memory alloys as new materials for aseismic isolation. J Eng Mech 1991;117(11):2590–608.
- [35] Liang C, Rogers C. A multi-dimensional constitutive model for shape memory alloys. J Eng Math 1992;26:429–43.
- [36] Brocca M, Brinson LC, Bazant ZP. Three-dimensional constitutive model for shape memory alloys based on microplane model. J Mech Phys Solids 2002;50(5):1051–77.
- [37] Zhang Y, Hu X, Zhu S. Seismic performance of benchmark base-isolated bridges with superelastic Cu–Al–Be restraining damping device. Struct Control Health Monit 2009;16:668–85.
- [38] Montecinos S, Cuniberti A, Sepúlveda A. Grain size and pseudoelastic behaviour of Cu–Al–Be alloy. Mater Charact 2008;59(2):117–23.
- [39] Marivil M. Superelastic behavior of CuAlBe alloy for earthquake engineer application. Mechanical Eng. Thesis. University of Chile; 2007 [in Spanish].
- [40] Gysling A. Numerical comparison of analytical models to predict cable behavior under axisymmetric loads. Civil Eng. Thesis. University of Chile; 2008 [in Spanish].
- [41] Beltran JF. Computational modeling of synthetic-fiber ropes. Ph.D. dissertation TX, USA: University of Texas at Austin. Austin; 2006.